Received: 9 July 2021 | Revised: 20 December 2021 | Accepted: 15 January 2022 | Published on: 11 February 2022
DOI: 10.1002/joc.7534

RESEARCH ARTICLE

International Journal of Climatology RMetS

Development of a wind and Pasquill stability class climate dataset for the North American Great Lakes region

Michael T. Kiefer[1] | Jeffrey A. Andresen[1] | Dale W. Rozeboom[2] | Xindi Bian[3]

[1]Department of Geography, Environment, and Spatial Sciences, Michigan State University, East Lansing, Michigan, USA
[2]Department of Animal Science, Michigan State University, East Lansing, Michigan, USA
[3]Northern Research Station, USDA Forest Service, Lansing, Michigan, USA

Correspondence
Michael T. Kiefer, Department of Geography, Environment, and Spatial Sciences, Michigan State University, 673 Auditorium Rd, Rm 116, East Lansing, MI 48824, USA.
Email: mtkiefer@msu.edu

Funding information
Michigan Alliance for Animal Agriculture, Grant/Award Number: AA16-008

[Correction added on 11 March 2022, after first online publication: The Acknowledgements section contains additional funding information.]

Abstract
In this study, a North American Regional Reanalysis (NARR)-based climate dataset of wind and Pasquill stability class is developed for the North American Great Lakes region. Motivated by the need to update the limited wind and Pasquill stability class climatology previously incorporated into a livestock odour nuisance-mitigation application used in Michigan, this study is motivated more generally by the lack of a long-term climate dataset suitable for studies of atmospheric dispersion in the Great Lakes region. As a preliminary step, NARR 10-m wind speed, 10-m wind direction, and 2-m temperature are evaluated at eight weather stations in Michigan and northern Indiana, and the wind speed variable is subsequently bias-corrected. To derive a Pasquill stability class dataset from the NARR variables, an existing empirical relationship between Pasquill stability class and Richardson number is applied to a previously developed NARR-derived Richardson number dataset covering the period 1979–2008. Pasquill stability class frequency in NARR is subsequently evaluated using observations at two flux towers in Illinois. Although a tendency is noted for the NARR-derived Pasquill stability class dataset to underestimate the frequency of stable and unstable conditions, and overestimate the frequency of neutral conditions, the analysis shows that the 10-m wind speed bias-correction procedure yields a frequency distribution that is in better agreement with the observations than the non-bias-corrected dataset. Finally, an analysis of the spatial and temporal variability of livestock odour dispersion potential in Michigan is provided as an example application of the NARR-based wind and Pasquill stability class climate dataset.

KEYWORDS
climatology, dispersion, Great Lakes, NARR, Pasquill stability, wind

1 | INTRODUCTION

Air flow in the atmosphere can be partitioned into three major components: (a) a slowly varying mean component; (b) a random, fluctuating turbulent component; and (c) a wave component (Stull, 1988). Regarding the movement of heat, moisture, and pollutants through the atmosphere, horizontal transport is largely a function of the mean component of the flow, and vertical transport is mainly attributable to the turbulent component of the flow (waves almost exclusively transport energy and momentum). Atmospheric dispersion is the spreading of pollutants from a source and is strongly influenced by the turbulent state of the atmosphere, which is in turn strongly influenced by static stability (Stull, 1988). Since static stability and turbulence are difficult to measure using standard observing systems, the Pasquill stability classification scheme (Pasquill, 1961) was developed to infer the ability of the atmosphere to disperse pollutants from standard surface weather observations. Different forms have been developed since the original 1961 study (Mohan and Siddiqui, 1998; Kahl and Chapman, 2018), but the most common form uses six stability classes, ordered from greatest to weakest dispersion potential: A (strongly unstable); B (moderately unstable); C (weakly unstable); D (neutral); E (weakly stable); F (strongly stable). The Pasquill stability classification scheme is used globally in dispersion applications where direct knowledge of turbulence is limited (e.g., Gryning and Lyck, 1984; Abdul-Wahab, 2006; Goldsmith Jr. *et al.*, 2012; Muthama *et al.*, 2015).

Methods for determining Pasquill stability class may be grouped into three broad categories (Mohan and Siddiqui, 1998; Kahl and Chapman, 2018), those that have the weakest physical basis, but are readily computed from standard weather station data [e.g., original Pasquill, 1961 method based on 10-m wind speed and either solar insolation (daytime) or cloud cover (nighttime)], those that have a somewhat stronger physical basis but that require measurements not typically available from station data [e.g., standard deviation of wind direction fluctuation, vertical temperature gradient, and wind speed ratio methods], and those that have the strongest physical basis but are generally too complicated and too restrictive in their requirements to be computed from station data [e.g., Obukhov length (L) and Richardson number (Ri) methods]. The two methods with the strongest physical basis are similar in that they compare the relative roles of shear production and buoyancy production/consumption terms in the equation for the rate of change of turbulent kinetic energy (TKE) (Stull, 1988). TKE is the mean kinetic energy per unit mass associated with eddies in turbulent flow and is a useful metric for evaluating the ability of the atmosphere to mix fresh air into, and thus dilute, the plume of pollutants emanating from a source. Knowledge of the propensity of the atmosphere to favour or oppose the development of turbulent eddies within the planetary boundary layer is the motivating factor for using such methods to diagnose Pasquill stability class. It is worth noting that Kahl and Chapman (2018) compared Pasquill stability classifications using the original Pasquill (1961) method to observed temperature lapse rates and found generally poor correspondence, lending support to the use of methods for diagnosing atmospheric stability and dispersion potential that have a stronger physical basis.

This study is motivated by two factors, one general and one specific. The general motivation for this study is the absence of a long-term climate dataset suitable for studies of atmospheric dispersion in the North American Great Lakes region (hereafter, Great Lakes region), a region with substantial terrain gradients, complex coastlines, and heterogeneous land surface types, and climates significantly modified by the presence of the Great Lakes (Andresen and Winkler, 2009). Such a dataset may be useful in studies of, for example, atmospheric stagnation, pollutant dispersion (including odours), insect and disease vector transport, and pollen dispersal. This is particularly true for a dataset capable of providing information about spatial as well as temporal variability of wind and Pasquill stability class.

The specific motivation for this study is the need to update the limited wind and Pasquill stability class climatology incorporated into the Michigan Odour from Feedlots Setback Estimation Tool (MI OFFSET, originally known as Michigan Odour Print; Person, 2000), a planning tool for assessing potential odour impacts from new or expanding livestock facilities in Michigan. MI OFFSET combines an empirical model of setback distance, defined as the distance downwind of an odour source where the odour intensity diminishes to a generally acceptable level, and a climatology of Pasquill stability class, wind speed, and wind direction, to yield a map of odour nuisance risk as a function of direction downwind of an odour source (known as an odour footprint). The empirical model was first developed for use in the predecessor of MI OFFSET, Minnesota OFFSET, using observations and dispersion model simulations of odour plumes at 85 livestock facilities in Minnesota (Guo *et al.*, 2005; Jacobson *et al.*, 2005). The developers of MI OFFSET used the United States Environmental Protection Agency–Support Center for Regulatory Atmospheric modeling (US EPA-SCRAM) surface meteorological data archive (1984–1992) (US EPA, 1993) to construct individual climatologies of Pasquill stability class, wind speed, and wind direction at eight weather station sites across Michigan and northern Indiana. A state-wide climatology of weather conditions favouring weak odour dispersion, and thus minimal dilution of odours, was then constructed by averaging the individual station climatologies (Person, 2000; Guo *et al.*, 2005).

In this study, the North American Regional Reanalysis (NARR) gridded dataset (Mesinger *et al.*, 2006) is chosen to replace the EPA-SCRAM dataset. NARR is a three-dimensional gridded atmospheric and land surface hydrology dataset covering North America and surrounding waters (Figure 1a), developed at the National Centers for Environmental Prediction (NCEP). NARR has been used previously in climatological studies of low-level jets (e.g., Doubler *et al.*, 2015), fire weather (e.g., Lu *et al.*, 2011), cold-air pools (e.g., Yu *et al.*, 2017), and wind energy (e.g., Li *et al.*, 2010). Of particular relevance to this study is a NARR-derived Ri climate dataset developed by Heilman and Bian (2013) as part of their climatological study of

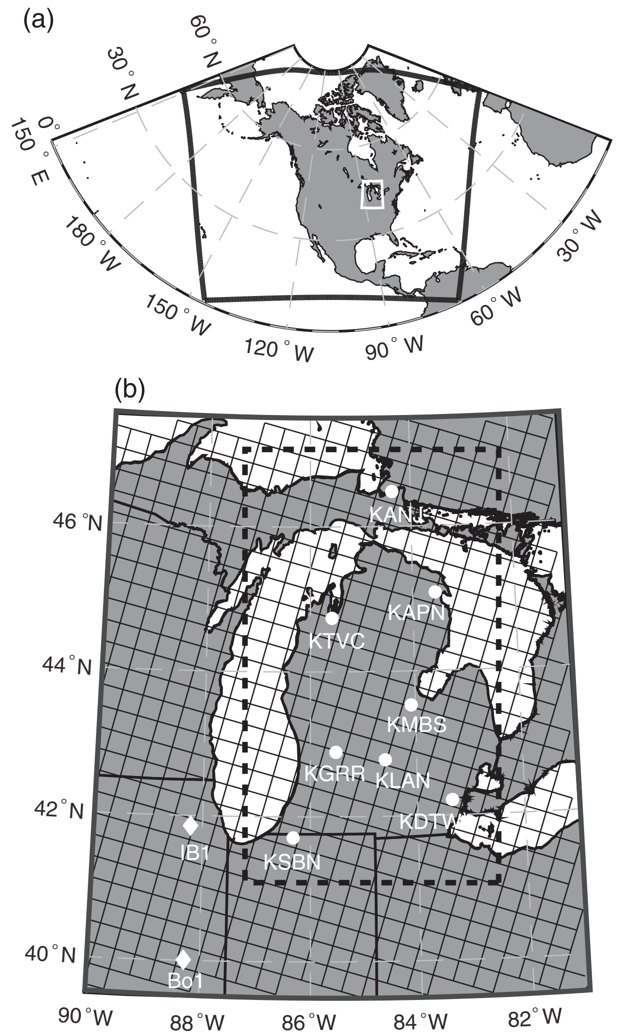

FIGURE 1 (a) Map of North America and surrounding waters, with the perimeter of the NARR domain indicated with a black rectangle, and the outline of the zoom panel (b) indicated with a white rectangle; (b) zoom panel showing a portion of the Great Lakes region centred on Michigan, with the NARR grid overlaid, and the locations of the automated weather stations used for the NARR variable assessment indicated with white circles (Table 1), and the locations of the two AmeriFlux towers used for the NARR Pasquill stability class dataset assessment indicated with white diamonds (Table 3). The dashed black rectangle in (b) depicts the analysis zone utilized in section 4; see Figure 5

conditions favouring erratic or extreme fire behaviour. This dataset is used in this study to derive a Pasquill stability class dataset. The approach taken in this study, applying a turbulence process-based method of diagnosing dispersion regimes to a bias-corrected gridded climate dataset to yield a gridded dataset of dispersion potential in the US Great Lakes region, is scientifically novel. To the authors' best knowledge, such an effort has not been undertaken previously. The aforementioned broad applicability of such a dataset, beyond the original motivation of odour dispersion, underscores the importance of this effort.

The objectives of this study are as follows. First, evaluate the potential for NARR to serve as the source for a wind and Pasquill stability class climate dataset for the Great Lakes region in general, and for use with MI OFFSET specifically, by assessing relevant NARR variables (10-m wind speed and direction, and 2-m temperature), and bias-correcting as needed. Second, diagnose Pasquill stability class from the Heilman and Bian (2013) NARR-derived *Ri* dataset (with *Ri* adjusted, if necessary, based on the outcome of the NARR variable assessment in step 1) and evaluate the resulting Pasquill stability class dataset. Third, integrate the new NARR-based wind and Pasquill stability class climate dataset in MI OFFSET (beyond the scope of this manuscript; not shown), and fourth, present an example application of the new climate dataset: an analysis of the spatial and temporal variability of odour dispersion potential in the Great Lakes region using the odour footprint output from MI OFFSET.

Although the focus of this study is on the Great Lakes region in general and Michigan specifically, it is expected that the method described here for analysing dispersion potential using a gridded climate dataset can be applied in other regions of the world. The setting for this study, a region with substantial terrain gradients, complex coastlines, and heterogeneous land use patterns, is not unique globally speaking. Other bodies of water with similarly complex physical geography include the Mediterranean and Black Seas (Eurasia), Russia's Lake Baikal (Eurasia), and Lake Victoria (Africa). The remainder of this manuscript is organized as follows. A description of the dataset development methodology is provided in section 2 (objectives 1–2), results and discussion of the dataset development process are provided in section 3 (objectives 1–2), an example application of the new climate dataset is presented in section 4 (objectives 3–4), and the paper is concluded in section 5.

2 | DATASET DEVELOPMENT: METHODOLOGY

2.1 | NARR background

NARR is the product of a data assimilation system that begins with 3-hr forecasts from the 32-km NCEP Eta model (Mesinger *et al.*, 1988; Janjić, 1994) as a first guess, and assimilates a suite of atmospheric observations to adjust the first guess toward observations. Observational datasets incorporated into NARR include rawinsonde, aircraft, surface station, and in situ and satellite-based sea-surface temperatures (including the Great Lakes).

NARR is produced on a grid with 32-km horizontal grid spacing and 45 vertical levels, and has a temporal frequency of 3 hr (eight files per day). NARR variables include, but are not limited to, the three wind components (west–east, south–north, vertical), potential temperature, relative humidity, surface sensible heat flux, accumulated precipitation, and sea level pressure.

Beyond the established utility of NARR for conducting climatological studies in North America, NARR was chosen to replace the EPA-SCRAM dataset for three reasons. First, NARR provides weather data on a regular 32-km grid, with the spacing between adjacent grid points smaller than the average spacing of weather stations in the EPA-SCRAM dataset (precise value unknown but at least as large as the 90 km average spacing of the higher-density Automated Surface Observing System (ASOS) network; Koch and Saleeby, 2001). Second, the NARR period of record begins on January 1, 1979, affording a much longer dataset than was available during the original development of MI OFFSET. A longer period of record minimizes the impact of any single year on statistics computed from the dataset, reducing the risk of bias from one or two unrepresentative years, and diminishing the impact of interannual variability. For this climatological source update to MI OFFSET, the 30-year period from January 1, 1979–December 31, 2008 is chosen. The choice of a 1979–2008 study period, as opposed to a more recent period (e.g., 1991–2020), is necessitated by our reliance on the Heilman and Bian (2013) NARR-derived *Ri* dataset as the starting point for the NARR-derived Pasquill stability class dataset. Third, NARR provides a larger suite of variables with which to work with, relative to the EPA-SCRAM dataset. This allows for the use of methods of determining Pasquill stability class other than the Pasquill (1961) 10-m wind speed–solar insolation/cloud cover method used in the original development of MI OFFSET, methods that in some cases have a more solid physical basis (e.g., *Ri*-based methods).

2.2 | NARR *Ri* formulation

In Heilman and Bian (2013), a form of flux *Ri* (Ri_f) compatible with NARR variables was utilized:

$$Ri_f = \frac{\frac{g}{\overline{\theta}}\overline{w'\theta'}}{\overline{u'w'}\frac{\partial \overline{U}}{\partial z} + \overline{v'w'}\frac{\partial \overline{V}}{\partial z}}, \tag{1}$$

where g is gravitational acceleration (m·s^{-2}), $\overline{\theta}$ is mean potential temperature (K), $\overline{w'\theta'}$ is sensible heat flux (K·m·s^{-1}), $\overline{u'w'}$ and $\overline{v'w'}$ are the zonal and meridional components of momentum flux, respectively (m^2·s^{-2}), and $\frac{\partial \overline{U}}{\partial z}$ and $\frac{\partial \overline{V}}{\partial z}$ are the vertical wind shears of the mean zonal and meridional wind components, respectively (s^{-1}).

The numerator and denominator in Equation (1) represent buoyancy production/consumption of TKE and shear production of TKE, respectively. The numerator was calculated using NARR standard output of surface sensible heat flux (H_S) and temperature at 2 m above ground level (AGL) (T_2). As the momentum fluxes in the denominator are not directly output from NARR, they were estimated from surface layer similarity theory using NARR standard output of wind speed at 10 m AGL (S_{10}). Hereafter, this form of Ri_f is referred to simply as *Ri*. The absence of any validation of the NARR *Ri* dataset or underlying NARR variables by Heilman and Bian (2013) motivated the following assessment.

2.3 | NARR variable assessment and bias-correction

An assessment of NARR S_{10}, 10-m wind direction (D_{10}), and T_2 was performed as a preliminary step in the development of the NARR-based wind and Pasquill stability class climate dataset. The other major variable used to compute NARR *Ri*, H_S, is not reported at automated weather stations; thus, it was not directly evaluated or bias-corrected. The limited number of studies that have examined NARR H_S (Monroe, 2007; Kumar and Merwade, 2011) suggest a tendency for NARR to overestimate it, particularly during the day. It is recommended that users of the NARR-based wind and Pasquill stability class climate dataset keep the largely unknown degree of H_S bias in NARR in mind. However, it is worth noting that previous NARR climatological studies directly related to atmospheric stability, for example, Lu *et al.* (2011) (fire weather) and Yu *et al.* (2017) (cold-air pools), did not report any concerns regarding NARR H_S.

For this assessment, hourly observations from eight automated weather stations in Michigan and Indiana (Figure 1b and Table 1) were obtained from the National Centers for Environmental Information (NCEI) Integrated Surface Database (ISD)-Lite (Smith *et al.*, 2011) for the 10-year period January 1, 1999–December 31, 2008. As seen in Table 1, the distance from each station site to the nearest Great Lake spans a broad range, from 10 km or less (KANJ, KAPN, and KTVC), to between 10 and 50 km (KDTW, KMBS, and KSBN), to 50 km or more (KLAN and KGRR). After isolating every third hourly (i.e., top-of-hour) observation (to match the 3-hourly NARR interval) and adjusting NARR wind speeds less than 1.3 m·s^{-1} (2.5 kt) to calm (to emulate ASOS reporting procedure; Nadolski, 1998), an evaluation of root-mean-square-error (RMSE) and mean bias error (MBE) was performed. For reference, ASOS hourly temperatures and wind speeds/directions are 5- and 2-min-average point observations, respectively, whereas NARR variables are instantaneous grid-volume averages; the reader is encouraged to keep these differences in mind when interpreting the results of the NARR variable assessment.

Finally, bias-correction of any NARR variable determined to exhibit substantial bias was performed by pooling the data at the eight stations, fitting a linear regression line to the points in a scatter plot figure (*x*-axis: NARR; *y*-axis: observation), and using the linear regression equation to adjust the NARR variable at every grid point and output timestep during the 1979–2008 study period.

2.4 | NARR Pasquill stability class derivation

An empirical relationship was used to diagnose Pasquill stability class from the NARR-derived *Ri* value (Table 2). The relationship was developed by Mohan and Siddiqui (1998) based on meteorological data collected during a 2-year field campaign at a coal-fired power plant in central Illinois. Mohan and Siddiqui (1998) related *Ri* and Pasquill stability class in a three step process wherein (a) *L* was computed from flux tower observations of air density, air temperature, friction velocity, and sensible heat flux; (b) *Ri* was computed from flux tower observations of air potential temperature and wind speed at two heights, and *Ri* was related to *L* using the relationship $Ri = (Z/L\phi_h)/\phi_m^2$, where *Z* is height AGL and ϕ_h and ϕ_m are nondimensional temperature and wind-profiles, respectively (also functions of *Z* and *L*); and (c) a look-up table of *L* threshold values and Pasquill stability class developed by Golder (1972) was used to relate *Ri* to Pasquill stability class. Mohan and Siddiqui (1998) concluded that schemes for diagnosing Pasquill stability class based on *L* or *Ri* were the best alternatives to the original Pasquill (1961) method based on S_{10}, solar insolation (daytime), and cloud cover (night-time). The reliance on similarity theory and empirical relationships notwithstanding, the use of a method to diagnose Pasquill stability class that considers turbulence processes increases our confidence in use of the NARR-derived Pasquill stability class dataset for dispersion applications.

2.5 | NARR Pasquill stability class assessment

As a final step in the dataset development process, we compared the NARR-derived Pasquill stability class dataset to a corresponding dataset derived from flux tower observations. As the intended use of the NARR dataset is climatological in nature, we chose to focus on the frequency distribution of Pasquill stability classes. Furthermore, as a means of assessing the impact of the NARR variable bias-correction procedure (section 2.3) on the calculation of Pasquill stability class, the frequency distribution of Pasquill stability class computed before and after the bias-correction was considered.

The use of sensible heat flux in the *Ri* buoyancy production/consumption term [numerator in Equation (1)] necessitated the use of data from flux towers, as opposed to data from standard surface weather stations that lack

TABLE 2 *Ri* limits for Pasquill stability classification, adapted from Table 3 in Mohan and Siddiqui (1998)

Pasquill stability class	Richardson number
A	$Ri \leq -5.34$
B	$-5.34 \leq Ri < -2.26$
C	$-2.26 \leq Ri < -0.569$
D	$-0.569 \leq Ri < 0.083$
E	$0.083 \leq Ri < 0.196$
F	$Ri \geq 0.196$

ICAO	City	Latitude	Longitude	Elevation	Distance
KANJ	Sault Ste. Marie	46.48	84.37	218	10
KAPN	Alpena	45.08	83.56	210	10
KDTW	Detroit	42.21	83.35	195	26
KGRR	Grand Rapids	42.89	85.52	237	57
KLAN	Lansing	42.78	84.59	264	115
KMBS	Saginaw	43.53	84.08	202	21
KSBN	South Bend	41.71	86.32	237	33
KTVC	Traverse City	44.74	85.58	190	2

TABLE 1 Metadata for eight automated surface weather stations utilized in this study: International Civil Aviation Organization (ICAO) identifier, nearest city, latitude (°N), longitude (°W), surface elevation (m), and approximate distance to the nearest Great Lake (including bays) (km; estimated using Google Earth; see Figure 1b for a map of the Great Lakes region with station locations overlaid)

flux instrumentation. Tower measurements at two AmeriFlux (http://ameriflux.lbl.gov/) tower sites in Illinois were used for this exercise: Bondville (Bo1) and Fermi Agricultural (IB1) (Figure 1b). The AmeriFlux network is a community of sites and scientists measuring ecosystem carbon, water, and energy fluxes across the Americas, and committed to producing and sharing high-quality eddy covariance data (Novick *et al.*, 2018). The sites were chosen for two reasons: first, the location of Bo1 and IB1 in central and northern Illinois, respectively, implies that they experience a climate comparable to Michigan and northern Indiana, where the S_{10} bias-correction was developed; second, the land use type at the two towers, cropland (as opposed to forest), means that the tower instrument heights (4.05 and 10 m AGL; Table 3) are comparable to the heights at which the NARR variables used to compute *Ri* are valid (surface, 2 m, and 10 m AGL). Metadata for the two towers is provided in Table 3, and the tower locations are displayed in Figure 1b. It is worth noting that although the NARR variables were evaluated at sites both upwind of and downwind of the Great Lakes (given a prevailing westerly to southwesterly wind; section 3.1) (Figure 1b, circles and Table 1), we evaluated the PRISM-derived Pasquill stability class dataset at sites exclusively upwind of the Great Lakes (Figure 1b, diamonds and Table 3). Alternative AmeriFlux sites in Michigan, Indiana, and Ohio were considered, but no nonforested sites immediately downwind of the Great Lakes were identified. The reader should keep this potential source of uncertainty in mind when interpreting the results of the NARR Pasquill stability class assessment, and when utilizing the resultant NARR-based wind and Pasquill stability class climate dataset.

3 | DATASET DEVELOPMENT: RESULTS AND DISCUSSION

3.1 | NARR variable assessment

Examining S_{10} at the eight ASOS station sites first, MBE was found to vary from as low as -0.2 m·s^{-1} at KMBS to as high as 1.9 m·s^{-1} at KTVC, with four stations exhibiting MBE magnitudes of 0.5 m·s^{-1} or smaller (KDTW, KGRR, KLAN, and KMBS), and three stations showing MBE at or above 1 m·s^{-1} (KAPN, KSBN, and KTVC). RMSE varied from as low as 1.6 m·s^{-1} at KDTW, KGRR, KLAN, and KMBS to as high as 2.8 m·s^{-1} at KAPN and KTVC. When observations from all eight stations were pooled together, the MBE and RMSE of the pooled dataset were 0.8 and 2.1 m·s^{-1}, respectively (for reference, mean observed S_{10} was 3.8 m·s^{-1}). NARR S_{10} MBE reported in the literature varies considerably and exhibits a regional dependence: Kennedy *et al.* (2011) reported MBE of about -1.6 m·s^{-1} at a site in the Southern Great Plains; Trubilowicz *et al.* (2016) reported MBE of 0.8–4.5 m·s^{-1} at three sites in southwestern British Columbia, Canada; Stegall and Zhang (2012) reported MBE between -3 and 3 m·s^{-1} across 140 sites in the North Slope region of Alaska. It is important to keep in mind that due to the sensitivity of near-surface wind to topography and land use, the surface wind speed MBE reported here is not necessarily representative of MBE in other regions of the NARR domain.

Proceeding to D_{10}, MBE varied from as low as $-0.4°$ at KDTW to as high as 11.3° at KAPN, and RMSE varied from as low as 29.6° at KLAN to as large as 45.5° at KANJ. The MBE and RMSE of the pooled dataset were 5.1° and 37.7°, respectively (for reference, mean observed D_{10} was 253.2°, that is, west-southwest). Previous assessments of NARR wind direction are much more limited than for wind speed, and restricted to assessment of random error, but Stegall and Zhang (2012) concluded that NARR adequately reproduced the variability of wind direction in their study domain (North Slope region of Alaska). When the high temporal and spatial variability of observed wind direction in the planetary boundary layer (Stull, 1988; Mahrt, 2011) is considered, the RMSE of 37.7° reported here appears reasonable.

Finally, examining T_2, MBE was found to vary from as low as -0.5°C at KGRR (i.e., cold bias) to as large as 0.7°C at KAPN (i.e., warm bias), and RMSE was found to vary in a relatively narrow range of 2.0–2.5°C. The MBE and RMSE for the pooled dataset were -0.1 and 2.2°C, respectively (for reference, mean observed T_2 was 8.7°C). The MBE reported here is within the range of previously reported NARR T_2 MBE: about 0.2°C at a site in the Southern Great Plains (Kennedy *et al.*, 2011); -0.1 to 0.5°C across four sites in southwestern British Columbia,

TABLE 3 Metadata for two AmeriFlux micrometeorological towers used in the NARR-derived Pasquill stability class assessment

ID	Name	Date range	Land use	% miss	$\overline{\theta}$	$\overline{w'\theta'}$	$\overline{U}$
Bo1	Bondvile	Aug 25, 1996–Apr 8, 2008	Cropland	16	10	10	10
IB1	Fermi Agric.	Mar 29, 2005–Dec 31, 2008	Cropland	14	4.05	4.05	4.05

Note: The last three columns indicate the height above the ground (m) at which potential temperature ($\overline{\theta}$), sensible heat flux ($\overline{w'\theta'}$), and wind speed ($\overline{U}$) were measured. See Figure 1b for a map of the Great Lakes region with tower locations overlaid.

Canada (Trubilowicz *et al.*, 2016); −1.4 to 1.7°C across 16 sites in the Mississippi River Basin (Kumar and Merwade, 2011).

Based on this assessment, we chose to bias-correct S_{10} only. This decision was made for two reasons. First, the MBE normalized by the mean observed value was considerably larger for S_{10} (21%) than for D_{10} (2%) or T_2 (−1%). Second, unlike the other NARR variables, wind speed impacts dispersion in more than one way, directly through transport and indirectly through turbulent mixing [via the conversion of kinetic energy from the mean flow to turbulent eddies; see denominator in Equation (1)].

3.2 | NARR wind speed bias-correction

The broad cloud of points in the eight-station pooled scatter plot in Figure 2, confirmed by the RMSE of 2.1 m·s^{-1} in Table 4, indicated considerable random error in the NARR estimates. This is in part attributable to the comparison of area-average gridded estimates to point observations. The MBE of 0.8 m·s^{-1} in Table 4 indicated a general tendency for NARR to overestimate S_{10}. When a linear regression line was fit to the data points (Figure 2), the resulting equation [$0.65198x + 0.77577$, where x is NARR S_{10}] confirmed the tendency for NARR to overestimate S_{10}. The regression line intersected the 1:1 line at NARR S_{10} = 2.2 m·s^{-1}, indicating that NARR S_{10} less than 2.2 m·s^{-1} tended to be too weak, and NARR S_{10} greater than 2.2 m·s^{-1} tended to be too strong.

Before proceeding, three points of clarification are necessary. First, it is important to keep in mind that we have compared area-average gridded estimates to point observations and an unknown portion of the gridded estimate—station observation difference can be attributed to spatial variability occurring at scales too small to be resolved by the 32-km grid. Second, analysis of the individual station error statistics (Table 4) revealed differences in the accuracy of NARR estimates between stations situated well inland (e.g., KLAN) and stations situated closer to the lakeshore (e.g., KTVC): accuracy was generally greatest at locations well inland and lowest at locations in closer proximity to the lakeshore. Analysis of linear regressions developed separately for inland and lakeshore station groups suggests that the bias-correction developed from the pooled data may overcorrect inland wind speeds and undercorrect lakeshore wind speeds (not shown). The pooling of lakeshore and interior station data prior to the bias-correction procedure is a source of uncertainty that should be kept in mind by users of the NARR-based wind and Pasquill stability class climate dataset. That said, pooling of the data was performed in the interest of generalizing the accuracy

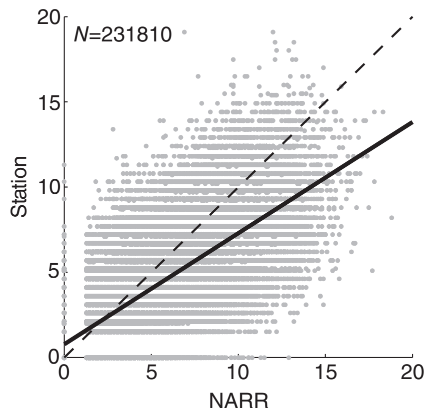

FIGURE 2 Scatter plot of NARR-estimated and station-observed S_{10} (m·s^{-1}) at eight automated weather stations (pooled). The dashed line is the 1:1 line and the thick line is the linear regression ($y = 0.65198x + 0.77577$); N is the number of data points. For station metadata and error statistics, see Tables 1 and 4, respectively

assessment and creating a one-size-fits-all bias-correction. Third, the restriction of the NARR variable assessment to eight stations in Michigan and northern Indiana implies that caution should be exercised when applying the resultant NARR-based wind and Pasquill stability class climate dataset in other regions of North America.

The linear regression equation was subsequently applied to NARR S_{10} at every grid point and every timestep, across the entire 30-year dataset. Following the adjustment of NARR S_{10} the MBE of the pooled dataset was eliminated, although bias at some stations increased (e.g., KMBS), or changed sign (e.g., KLAN). With the caveat that this assessment was performed with the same station dataset used to develop the regression equation, the reduction in overall MBE increased confidence in our use of NARR to develop a wind and Pasquill stability class climate dataset.

As a final step in the bias-correction procedure, the NARR-derived *Ri* dataset from Heilman and Bian (2013) was adjusted to reflect the effect of the bias-correction on the shear production term (denominator in Equation (1) is a function of S_{10}). Thus, the S_{10} bias-correction impacted the NARR-based wind and Pasquill stability class climate dataset in two ways: directly (S_{10}) and indirectly (*Ri*). Lastly, a word of caution is necessary regarding the applicability of the dataset. Because the S_{10} bias-correction was based on data from weather stations sited in Michigan and northern Indiana, and the assessment of the NARR-derived Pasquill stability class dataset was performed with data from flux tower sites in northern Illinois (section 3.3), confidence in the accuracy of the NARR-based wind and Pasquill stability class climate dataset diminishes with distance from the area comprising Michigan and the northern portions of Indiana and Illinois (Figure 1b).

TABLE 4 Summary statistics for NARR 10-m wind speed (S_{10}; m·s^{-1}), 10-m wind direction (D_{10}; degree), and 2-m temperature (T_2; °C) at the eight automated weather stations listed in Table 1 and shown in Figure 1b: sample size (N), mean bias error (MBE: NARR-station), and root-mean-square error (RMSE)

	S_{10}			D_{10}			T_2		
ICAO	N	MBE	RMSE	N	MBE	RMSE	N	MBE	RMSE
KANJ	29092	0.8	2.0	23697	7.9	45.5	29167	0.3	2.2
KAPN	29011	1.8	2.8	22916	11.3	41.6	29166	0.7	2.5
KDTW	29029	0.2	1.6	24887	−0.4	33.9	29182	−0.4	2.1
KGRR	29106	0.2	1.6	25480	7.4	34.9	29186	−0.5	2.0
KLAN	29148	0.5	1.6	24280	5.2	29.6	29187	−0.3	2.2
KMBS	28566	−0.2	1.6	24407	−0.3	33.2	28629	0.2	2.2
KSBN	29152	1.2	2.3	24469	7.6	38.1	29192	−0.2	2.0
KTVC	28706	1.9	2.8	18531	2.3	44.3	28961	−0.3	2.3
Pooled	231810	0.8	2.1	188667	5.1	37.7	232670	−0.1	2.2

Note: N is smaller for D_{10} than S_{10} due to the occurrence of calm winds, wherein D_{10} is undefined.

3.3 | NARR Pasquill stability class assessment

Lastly, the Mohan and Siddiqui (1998) empirical relationship (Table 2) was used to diagnose Pasquill stability class from NARR-derived Ri, and the resulting Pasquill stability class dataset was evaluated. In Figure 3, the frequency distribution of unstable (A, B, and C; combined), neutral (D), weakly stable (E), and strongly stable (F) classes is shown for the AmeriFlux tower-derived (T) and NARR-derived (Nb: before S_{10} bias-correction; Na: after S_{10} bias-correction) Pasquill stability class datasets. Examining frequency distributions of the tower-derived dataset first, observed frequencies at the two towers were found to differ by less than 3%. Strongly stable conditions occurred most frequently (F: 41.5–44.4%), followed by unstable (A, B, and C: 27.0–29.4%), neutral (D: 23.0–24.2%) and weakly stable (4.9–5.5%) conditions. Comparing the frequency distributions of the NARR-derived dataset before and after the S_{10} bias-correction to the tower-derived dataset, the bias-correction was found to have a positive impact on the NARR assessment. Before the bias-correction, the most frequent class was D (neutral), however, after bias-correction the most frequent class was F (strongly stable), in agreement with the tower data. Furthermore, after the bias-correction the NARR- and tower-derived Pasquill class frequencies were found to differ by at most 6.8% (class F). Although NARR was found to still overestimate the frequency of classes D and E, and underestimate the frequency of classes A, B, C, and F, the bias-corrected NARR dataset did reproduce the observed Pasquill stability class frequency distribution in northern Illinois.

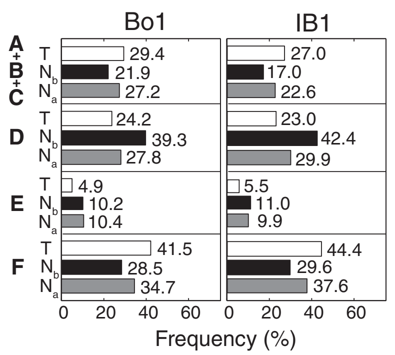

FIGURE 3 Frequency of Pasquill stability classes A, B, and C (unstable; grouped), D (neutral), E (weakly stable), and F (strongly stable), at AmeriFlux towers Bo1 and IB1; see tower metadata in Table 3. In each panel, the top bar corresponds to the tower observations (T; white), the middle bar corresponds to NARR before the S_{10} bias-correction (N_b; black), and the bottom bar corresponds to NARR after the S_{10} bias-correction (N_a; grey)

4 | EXAMPLE APPLICATION

4.1 | MI OFFSET background

In this section we present an example application of the NARR-based wind and Pasquill stability class climate dataset: an analysis of the spatial and temporal variability of livestock odour dispersion potential across Michigan and the surrounding Great Lakes. The MI OFFSET livestock facility siting application and its primary output the odour footprint is utilized for this purpose. However, the state-wide climatology of wind and Pasquill stability class, based on data from eight weather stations in the 9-year EPA-SCRAM dataset (Person, 2000), is replaced with 30-year NARR-based climatologies at each grid point. Note that in the following discussion, "OFFSET" is used when referring generally to the OFFSET framework (common to Minnesota and MI OFFSET), and "MI OFFSET" is used when referring specifically to the Michigan application. Recall from section 1 that the odour footprint is a plan-view graphic of setback distance (d) as a function of direction downwind of a point odour source, where d is defined as the distance needed between source and receptor for odour intensity at the receptor to be acceptable to the general population approximately N% of the time (where N is a confidence level, generally between 91 and 99). An "acceptable" odour intensity is defined in OFFSET as an odour intensity of 2 or less on a 0–5 n-butanol reference scale (faint odour), equivalent to an odour concentration of 75 odour units (OU) m^{-3} (an air sample collected at distance d from the source would need to be mixed with a volume of fresh air 75 times the volume of the original air sample for the odour to be undetectable to 50% of the general population) (Guo *et al*., 2005; Jacobson *et al*., 2005).

The odour-annoyance frequency (f_o), equivalent to $1 - N$, is closely related to the frequency of weather conditions favourable for weak odour dispersion, that is, light winds and stable stratification. In OFFSET, six weather conditions are defined that combine Pasquill stability class (representing the potential for turbulent mixing) and S_{10} (representing the potential for mean transport). Ordered from least dispersive to most dispersive, the conditions are WC1 [F; $S_{10} \leq 1.3$ m·s^{-1}], WC2 [F; 1.3 m·s$^{-1} < S_{10} \leq 3.1$ m·s^{-1}], WC3 [E; $S_{10} \leq 3.1$ m·s^{-1}], WC4 [E; 3.1 m·s$^{-1} < S_{10} \leq 5.4$ m·s^{-1}, WC5 [D; $S_{10} \leq 5.4$ m·s^{-1}], and WC6 [D; 5.4 m·s$^{-1} < S_{10} \leq 8.0$ m·s^{-1}] (Jacobson *et al*., 2005). As an unstable atmosphere (Pasquill stability classes A–C) is likely to result in rapid turbulent mixing of odorous and nonodorous air, d is only computed for Pasquill stability classes D–F. An empirical relationship is used to compute d, $d = ae^b$, where e is total odour emission factor (a measure of odour source strength), and a and b are weather influence factors that represent the combined effect of mean transport and turbulent mixing on odour dispersion. This empirical relationship was developed from field observations and dispersion model simulations of odour plumes in Minnesota (Guo *et al*., 2005; Jacobson *et al*., 2005), but was assumed by Person (2000) to be applicable to Michigan livestock facilities as well. For each of sixteen 22.5°-wide wind direction bins, the cumulative frequency of each weather condition (frequency of that condition plus the frequency of less dispersive conditions) is examined. The weather condition whose cumulative frequency comes closest to, without going over, the desired f_o is identified, and the weather influence factors for that condition are used, along with e, to compute d. The process is then repeated for the remaining wind direction bins, yielding the odour footprint.

The 5% odour footprint (i.e., $f_o = 5$) is used by the Michigan Department of Agriculture and Rural Development (MDARD) in approving siting plans for farms requesting legal protection against future odour nuisance complaints associated with new or expanded livestock facilities (in accordance with Michigan's Right-to-Farm Act). Farms whose siting plans are approved are then protected from future odour-nuisance lawsuits from neighbours located outside the footprint (i.e., beyond d, where odour nuisance frequency less than 5% is expected). In the odour footprint schematic provided in Figure 4, the odour footprint for the hypothetical barn indicates that the state would extend to the owner of the barn legal protection against odour nuisance lawsuits from neighbours 1–4, but not from neighbour 5.

4.2 | Spatial variability

In Figures 5, 5% odour footprints are displayed at all NARR grid points over Michigan and the surrounding Great Lakes (Figure 5a), along with corresponding wind rose shapes colour-coded by the frequency of $S_{10} \leq 5.4$ m·s^{-1} (Figure 5b), and the frequency of the three general Pasquill stability categories, unstable (classes A–C), neutral (class D), and stable (classes E–F) (Figure 5c). For reference, a wind rose is a diagram depicting the relative frequency of a wind direction for any number of wind direction bins around the compass;

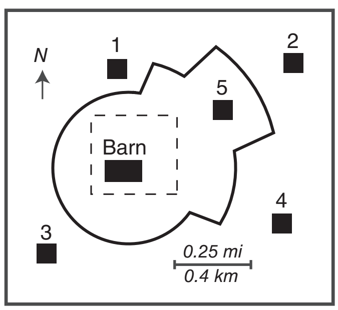

FIGURE 4 Odour footprint schematic for a barn to be constructed inside the hypothetical farm parcel denoted with the dashed square. Neighbours 1–4 are located outside the 5% odour footprint and are expected to be free from noticeable odours more than 95% of the time, whereas neighbour 5 is located inside the 5% odour footprint and is expected to be free from noticeable odours less than 95% of the time. This scenario would result in the state extending to the owner of the farm parcel legal protection against odour nuisance lawsuits related to the barn from neighbours 1–4, but not from neighbour 5

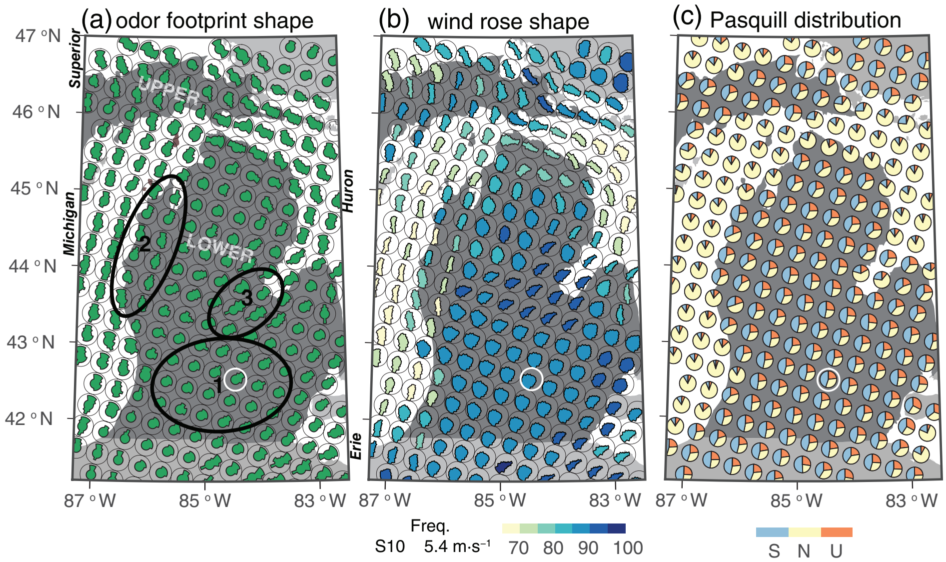

FIGURE 5 Maps of (a) 5% odour footprint shape; (b) wind rose shape, with frequency of $S_{10} \leq 5.4$ m·s^{-1} indicated by colour shading; and (c) distribution of unstable (A, B, and C), neutral (d), and stable (E and F) Pasquill stability categories, developed using all hours in the NARR-based climatology of wind and Pasquill stability class. See Figure 1 for location of analysis zone within broader NARR domain. In (a), an arbitrarily large odour source strength is used to make the footprints visible from a great distance. Land areas are shaded grey (Michigan denoted with dark grey shading; upper and lower peninsulas labelled), bodies of water are shaded white, and Great Lakes are labelled in (a). Labelled black ovals in (a) indicate footprint shape categories discussed in text, and the white circle in each panel indicates the grid point selected for analysis of temporal variability in Figure 6

each wind rose shape in Figure 5b is created by normalizing the wind rose, constructed using 22.5°-wide bins, by the compass-maximum frequency. The 5.4 m·s^{-1} wind speed threshold appears in the OFFSET weather conditions WC4, WC5, and WC6, and is used in this section to examine spatial and temporal variability of wind speeds favouring odour transport. Note also that in Figure 5a, an arbitrarily large odour source strength is used to make the footprints visible from a great distance; thus, only relative magnitudes of d are meaningful. For a given location, odour footprint shape provides information about the preferred direction(s) for odour dispersion, and odour footprint area (i.e., d integrated around the compass) is an indicator of the overall magnitude of odour nuisance risk.

Two broad statements can be made based on a brief examination of Figure 5a. First, footprint shape and area differ considerably between lake and land grid points. Footprints over the lakes are generally larger than their overland counterparts and tend to be aligned with the lake (e.g., south-southwest to north-northeast orientation for footprints over Lake Michigan, west-northwest to east-southeast orientation for footprints over northern Lake Huron). Second, footprint shapes over land tend to fall into one of several common categories (denoted by black ovals in Figure 5a), including (a) "interior Lower Peninsula" (round footprint with southwest–northeast orientation), (b) "northwest Lower Peninsula" (narrow footprint with south-southwest to north-northeast orientation), and (c) "Saginaw Valley" (wedge-shaped footprint with southwest–northeast orientation; named after Saginaw Bay, northeast of oval #3). It should be emphasized that this study is, to the best of our knowledge, the first to examine spatial patterns of odour dispersion potential across Michigan and the Great Lakes region in general.

To provide some explanation for the odour footprint patterns seen in Figure 5a, analysis now proceeds to maps of wind rose shape and Pasquill stability class frequency (Figure 5b,c). First, note the close correspondence between odour footprint shape in Figure 5a and wind rose shape in Figure 5b. The orientation of the wind roses closely parallels that of the footprints, albeit with directions reversed (wind rose: direction wind is blowing *from*; footprint: direction odour is dispersed *toward*), and the narrowness or broadness of the wind roses also parallels that of the odour footprints. Second, observe that the frequency of $S_{10} \leq 5.4$ m·s^{-1} is noticeably lower over the lakes (generally 65–80%, compared to 80–95% over land), consistent with the higher frequency of the neutral stability category over the lakes (80–90%, compared to 35–50% over land; Figure 5c). Finally, note the more equitable frequency distribution of the neutral, stable, and unstable categories over land, albeit with the stable category generally occurring most frequently (Figure 5c).

Although a thorough examination of the underlying processes behind the odour footprint map in Figure 5a is beyond the scope of this manuscript, the generally larger 5% odour footprint areas over water can be attributed to a higher frequency of neutral Pasquill stability class D there: for a given wind direction, the cumulative frequencies of the two weather conditions with Pasquill stability class D (WC5 and WC6) each exceed 5%, meaning that the less frequent and slightly less dispersive WC4 (with larger a and b coefficients, and thus larger d) is chosen as the 5% class.

The impact of the Great Lakes on the climatologies of wind speed, wind direction, and atmospheric stability over and downwind of the lakes, and consequently the climatology of dispersion potential, is clear. The differences in climatologies between over-lake, lakeshore, and inland locations are broadly consistent with the findings gleaned by Changnon Jr. and Jones (1972) from widely spaced weather station data. However, the complex spatial patterns seen in Figure 5 are virtually impossible to discern through analysis of station data alone. Gridded datasets like NARR allow for a more complete picture of the spatial variability of climate in the Great Lakes region than is possible from point observations.

4.3 | Temporal variability

In Figure 6, time series of 5% footprint area, frequency of $S_{10} \leq 5.4$ m·s^{-1}, and frequency of the three general Pasquill stability categories (unstable, neutral, and stable) are presented, with data segregated by month and by hour; data are extracted at the grid point denoted by the white circle in Figure 5. Beginning with the time series of footprint area segregated by month (Figure 6a), note the presence of an annual cycle, consisting of two maxima (December/January: 1.5 km^2; July/August: 1.4 km^2) and two minima (May: 0.8 km^2; September: 0.9 km^2). Over the course of the year, footprint area varies across a 0.7 km^2 range, or about 58% of the annual mean (1.2 km^2).

Proceeding to the time series of the frequency of $S_{10} \leq 5.4$ m·s^{-1} segregated by month (Figure 6c), we find an annual cycle resembling a bell curve, with a peak in August ($S_{10} \leq 5.4$ m·s^{-1} ~97.5% of the time), flanking transition periods during April–August and August–November, and a "tail" of relatively constant frequency from November to April ($S_{10} \leq 5.4$ m·s^{-1} ~83% of the time). It is important to note that the annual cycle of the frequency of $S_{10} \leq 5.4$ m·s^{-1} parallels that of the poleward migration of the jet stream in spring and equatorward migration in autumn (not shown). The time series of Pasquill stability category frequency (Figure 6e) shows nearly mirror-image annual cycles for neutral and unstable categories, with maximum and minimum neutral category frequency occurring in January and August, respectively, and maximum and minimum unstable category frequency occurring in August and December, respectively. In contrast, maximum and minimum stable category frequency occurs in September and March, respectively. The annual range in frequency (maximum–minimum) is about the same for the neutral and unstable categories (~30%), while the annual range is smaller for the stable category (~10%).

Taken together, the left-hand panels in Figure 6 suggest a relationship between the annual cycle of 5% footprint area and the annual cycles of wind speed and Pasquill stability category frequency. The peak in footprint area in July and August (Figure 6a) coincides with the annual peak in the frequency of $S_{10} \leq 5.4$ m·s^{-1} in August (Figure 6c) and a period of higher stable category frequency from July to October (with the aforementioned peak in September; Figure 6e); thus, weather conditions that are most favourable for weak odour dispersion and enlarged odour footprints (light winds and/or stable atmosphere) are more frequent in July and August than in the flanking months. In contrast, the peak in footprint area in December and January (Figure 6a) occurs during a six-month period when the frequency of $S_{10} \leq 5.4$ m·s^{-1} varies little from month-to-month and is 10–15% lower than during the summer (Figure 6c). It appears that the winter peak in 5% footprint area is related to the annual cycle of combined neutral and stable category frequency, as the annual maximum occurs in December and January as well (Figure 6e). Recall that in OFFSET, d is only computed for the stable and neutral Pasquill stability categories, as rapid odour dispersion via turbulent mixing is expected for the unstable category.

Proceeding to the time series of 5% footprint area segregated by hour (Figure 6b), note the presence of a diurnal cycle consisting of a pre-sunrise maximum of 2.2 km^2 at 0900 UTC [0500 eastern daylight time (EDT = UTC − 4)] and a late-morning minimum of 0.8 km^2 at 1500 UTC (1100 EDT). Over the course of a 24-hr period, footprint area varies across a 1.4 km^2 range, or about 93% of the daily mean (1.5 km^2). Thus, the magnitude of diurnal variability is considerably greater than the magnitude of seasonal variability (cf., Figure 6a,b). Examining the time series of the frequency of $S_{10} \leq 5.4$ m·s^{-1} next (Figure 6d), a diurnal cycle is found with the highest frequency during the overnight period [0600–1200 UTC (0200–0800 EDT)] and the lowest frequency during the afternoon [1800–2100 UTC (1400–1700 EDT)].

Evaluating the time series of Pasquill stability category frequency last (Figure 6f), the diurnal cycles of stable and unstable category frequency are found to largely mirror each other. Stable category frequency is highest

FIGURE 6 Time series of (a, b) 5% footprint area, (c, d) frequency of $S_{10} \leq 5.4$ m·s^{-1}, and (e, f) frequency of unstable (classes A–C; dotted line with squares), neutral (class D; dashed line with unfilled circles), and stable (classes E, F; solid line with filled circles) Pasquill stability categories. In the left (right) panels, the NARR-based wind and Pasquill stability class climate dataset is segregated by month (hour); time is indicated in UTC and eastern daylight time (EDT: UTC − 4). Data for the time series were extracted at the grid point denoted by the white circle in Figure 5. For computing footprint area, a total odour emission factor (e; section 4) of 136 was utilized, appropriate for a 3,716 m^2 (40,000 ft^2) finishing swine barn. For a visualization of a hypothetical application of the odour footprint analysed in this figure, see the schematic in Figure 4

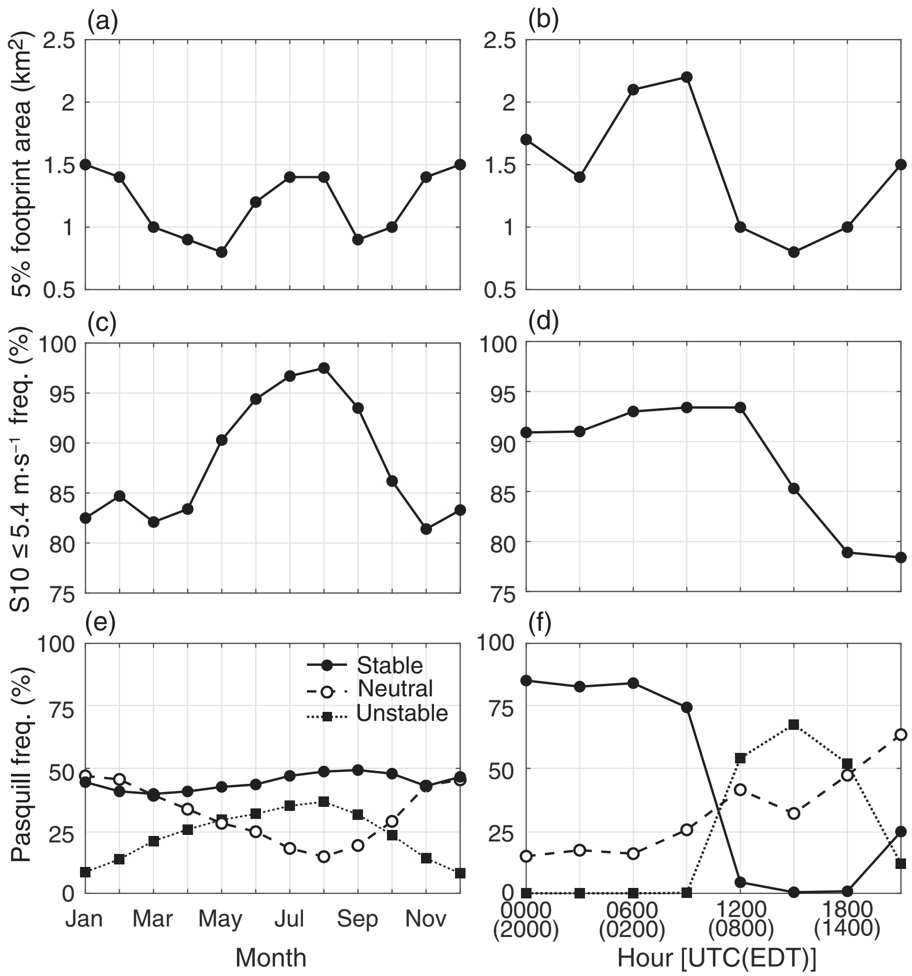

from 0000–0900 UTC (2000–0500 EDT) and lowest from 1200 to 1800 UTC (0800–1400 EDT); unstable category frequency is highest from 1200–1800 UTC (0800–1400 EDT) and lowest from 0000–0900 UTC (2000–0500 EDT). Meanwhile, the diurnal cycle of neutral stability largely mirrors the diurnal cycle of wind speed (Figure 6d), with the highest frequency of neutral stability at 2100 UTC (1700 EDT), when the frequency of $S_{10} \leq 5.4$ m·s^{-1} is at the diurnal minimum. It is interesting to note that the peak in unstable category frequency does not occur during peak heating (mid-afternoon) but occurs during the late morning/early afternoon period when the mixed layer is growing and near-surface wind speeds are increasing but have not reached their afternoon peak. Knowledge of the diurnal cycle of dispersion potential afforded by this new dataset may have practical applications; for example, a farmer might use knowledge of the timing of peak unstable category frequency to minimize the disturbance of nearby residential neighbourhoods from the application of fertilizer to their fields or the seasonal burning of crop residue.

Taken as a whole, the right-hand panels in Figure 6 indicate that the pre-sunrise maximum in 5% footprint area (Figure 6b) is related to both the diurnal maximum in the frequency of $S_{10} \leq 5.4$ m·s^{-1} (Figure 6d) and the diurnal maximum in stable category frequency (Figure 6f), and the late morning minimum in 5% footprint area (Figure 6b) is related to both the late-morning decreasing trend in the frequency of $S_{10} \leq 5.4$ m·s^{-1} (Figure 6d) and the diurnal minimum in stable category frequency (Figure 6f).

5 | SUMMARY AND CONCLUSIONS

In this study, a NARR-based climate dataset of wind and Pasquill stability class has been developed for the North American Great Lakes region. Covering the period from 1979 to 2008, the dataset was developed due to both the lack of a long-term climate dataset suitable for studying atmospheric dispersion potential in the Great Lakes region, and the need to update the wind and Pasquill stability class climate dataset incorporated into the livestock odour siting tool, MI OFFSET. The approach taken in this study, applying a turbulence process-based method of diagnosing dispersion regimes (*Ri* method) to a bias-corrected gridded climate dataset (NARR) to yield a gridded dataset of dispersion potential in the US Great Lakes region, has not been undertaken previously. The stated objectives of this study were as follows: first, evaluate the potential for NARR to serve as the source for a wind and Pasquill stability class climate dataset for the Great Lakes region in general, and for use in MI OFFSET specifically; second, diagnose Pasquill stability class from the Heilman and Bian (2013) NARR-derived *Ri* dataset, and evaluate the resulting Pasquill stability class dataset; third, integrate the new NARR-based wind and Pasquill stability class climate dataset into MI OFFSET (outside scope of manuscript; not shown); and fourth, analyse the spatial and temporal variability of odour dispersion potential in the Great Lakes region using the odour footprint output from MI OFFSET.

The first step taken was to evaluate NARR S_{10}, D_{10}, and T_2 at eight automated weather station sites in Michigan and northern Indiana. The analysis revealed that MBE normalized by the mean observed value was considerably larger for S_{10} than for D_{10} and T_2 (21 vs. 2 and −1%, respectively). For this reason, and because wind speed influences dispersion in two ways (directly, via mean transport, and indirectly, via turbulent mixing), a decision was made to bias-correct S_{10} only. Thus, S_{10} was bias-corrected and the Heilman and Bian (2013) NARR-derived *Ri* dataset was adjusted to account for the S_{10} bias incorporated into the original *Ri* dataset. Following the bias-correction, Pasquill stability class was derived from *Ri* using an empirical relationship developed by Mohan and Siddiqui (1998). Next, Pasquill stability class frequency was compared between observations at two AmeriFlux tower sites in northern Illinois, and NARR-derived estimates at the nearest grid points to the two towers. Although a tendency was noted for NARR to underestimate the frequency of stable and unstable conditions, and overestimate the frequency of neutral conditions, the analysis showed that the S_{10} bias-correction procedure improved the comparison and yielded a more realistic frequency distribution. Finally, an example application of the NARR-based wind and Pasquill stability class climate dataset was presented—an analysis of the spatial and temporal variability of odour dispersion potential across Michigan and the surrounding Great Lakes. Footprint shape and area were found to differ considerably between lake and land grid points, with footprints over the lakes tending to be larger than their overland counterparts, and generally aligned with the lakes. Such spatial patterns are virtually impossible to diagnose through analysis of station data alone. Lastly, time series of footprint area segregated by month exhibited winter/summer maxima and spring/autumn minima, and corresponding time series segregated by hour exhibited a pre-sunrise maximum and a late-morning minimum.

The outcome of this study is a climate dataset with a broad range of possible applications, including but not limited to, studies of atmospheric stagnation, pollutant dispersion (including odours), insect and disease vector transport, and pollen dispersal. Although the focus of this study was regional in nature, it is expected that the method developed herein for analysing spatial and temporal variability of dispersion potential in areas with complex physical geography can be extended to gridded datasets in other regions of the world. However, it is important to note the limitations of this dataset. First, confidence in the accuracy of the dataset outside of Michigan and the northern portions of Indiana and Illinois is limited, since the S_{10} bias-correction procedure was based on data from weather stations in Michigan and northern Indiana, and the Pasquill stability class dataset assessment was performed using flux tower data from sites in central and northern Illinois. Second, the limited knowledge of NARR H_S bias contributes to some uncertainty regarding the accuracy of the NARR-derived Pasquill stability class dataset, since the *Ri* dataset used to compute Pasquill stability class is itself a function of NARR H_S. Third, the use of the Heilman and Bian (2013) NARR-derived *Ri* dataset in the development of the NARR-based wind and Pasquill stability class dataset constrained the study period to 1979–2008. An update to the dataset to incorporate more recent years is planned for future work. Finally, the NARR grid spacing (32 km) limits the applicability of the wind and Pasquill stability class climate dataset to the meso-beta scale (20–200 km) or larger. Despite these limitations, the new NARR-based wind and Pasquill stability class climate dataset has the potential to be a useful tool for future climatological studies in the Great Lakes region.

ACKNOWLEDGEMENTS

This work was supported by the Michigan Alliance for Animal Agriculture (Grant # AA16-008) and Michigan State University AgBioResearch (Project # MICL02548) The colour maps used in Figure 5b,c were developed by Cynthia Brewer, at the Pennsylvania State University (https://colorbrewer2.org/). Finally, comments and suggestions from the Associate Editor and two anonymous reviewers were helpful in revising the manuscript and are greatly appreciated.

AUTHOR CONTRIBUTIONS

Michael T. Kiefer: Conceptualization; data curation; formal analysis; investigation; methodology; validation; visualization; writing – original draft; writing – review and editing. **Jeffrey A. Andresen:** Conceptualization;

formal analysis; investigation; methodology; project administration; resources; supervision; writing – review and editing. **Dale W. Rozeboom:** Project administration; resources; writing – review and editing. **Xindi Bian:** Methodology; resources; writing – review and editing.

DATA AVAILABILITY STATEMENT

The NARR-based wind and Pasquill stability class climate dataset (along with accompanying metadata) has been uploaded to the Harvard Dataverse (Kiefer et al., 2022).

ORCID

Michael T. Kiefer https://orcid.org/0000-0002-4824-0148

REFERENCES

Abdul-Wahab, S.A. (2006) Impact of fugitive dust emissions from cement plants on nearby communities. *Ecological Modelling*, 195, 338–348. https://doi.org/10.1016/j.ecolmodel.2005.11.044.

Andresen, J.A. and Winkler, J.A. (2009) Weather and climate. In: Schaetzl, R.J., Brandt, D. and Darden, J.T. (Eds.) *Michigan Geography and Geology*. Boston, MA: Pearson Custom, pp. 288–314.

Changnon, S.A., Jr. and Jones, D.M.A. (1972) Review of the influences of the Great Lakes on weather. *Water Resources Research*, 8, 360–371.

Doubler, D.L., Winkler, J.A., Bian, X., Walters, C.K. and Zhong, S. (2015) An NARR-derived climatology of southerly and northerly low-level jets over North America and coastal environs. *Journal of Applied Meteorology and Climatology*, 54, 1596–1619.

Golder, D. (1972) Relation among stability parameter in the surface layer. *Boundary-Layer Meteorology*, 13, 47–58.

Goldsmith, C.D., Jr., Chanton, J., Abichou, T., Swan, N., Green, R. and Hater, G. (2012) Methane emissions from 20 landfills across the United States using vertical radial plume mapping. *Journal of the Air & Waste Management Association*, 62, 183–197. https://doi.org/10.1080/10473289.2011.639480.

Gryning, S.-E. and Lyck, E. (1984) Atmospheric dispersion from elevated sources in an urban area: comparison between tracer experiments and model calculations. *Journal of Climate and Applied Meteorology*, 23, 651–660. https://doi.org/10.1175/1520-0450(1984)023<0651:ADFESI>2.0.CO;2.

Guo, H., Jacobson, L.D., Schmidt, D.R., Nicolai, R.E., Zhu, J. and Janni, K.A. (2005) Development of the OFFSET model for determination of odor-annoyance-free setback distances from animal production sites: part II. Model development and evaluations. *Transactions of the ASAE*, 48, 2269–2276.

Heilman, W.E. and Bian, X. (2013) Climatic variability of near-surface turbulent kinetic energy over the United States: implications for fire-weather predictions. *Journal of Applied Meteorology and Climatology*, 52, 753–772.

Jacobson, L.D., Guo, H., Schmidt, D.R., Nicolai, R.E., Zhu, J. and Janni, K.A. (2005) Development of the OFFSET model for determination of odor-annoyance-free setback distances from animal production sites: part I. review and experiment. *Transactions of the ASAE*, 48, 2259–2268.

Janjić, Z.I. (1994) The step-mountain Eta coordinate model: further developments of the convection, viscous sublayer, and turbulence closure schemes. *Monthly Weather Review*, 122, 927–945.

Kahl, J.D.W. and Chapman, H.L. (2018) Atmospheric stability characterization using the Pasquill method: a critical evaluation. *Atmospheric Environment*, 187, 196–209. https://doi.org/10.1016/j.atmosenv.2018.05.058.

Kennedy, A.D., Dong, X., Xi, B., Xie, S., Zhang, Y. and Chen, J. (2011) A comparison of MERRA and NARR reanalyses with the DOE ARM SGP data. *Journal of Climate*, 24, 4541–4557. https://doi.org/10.1175/2011JCLI3978.1.

Kiefer, M. T., J. A. Andresen, D. W. Rozeboom & X. Bian (2022) NARR-based wind and Pasquill stability class climate dataset [Data set], V1, Harvard Dataverse. https://doi.org/10.7910/DVN/ZT5NGK.

Koch, S.E. and Saleeby, S. (2001) An automated system for the analysis of gravity waves and other mesoscale phenomena. *Weather Forecasting*, 16, 661–679. https://doi.org/10.1175/1520-0434(2001)016<0661:AASFTA>2.0.CO;2.

Kumar, S. and Merwade, V. (2011) Evaluation of NARR and CLM3.5 outputs for surface water and energy budgets in the Mississippi River basin. *Journal of Geophysical Research*, 116, D08115.

Li, X., Zhong, S., Bian, X. and Heilman, W.E. (2010) Climate and climate variability of the wind power resources in the Great Lakes region of the United States. *Journal of Geophysical Research*, 115, D18107.

Lu, W., Charney, J.J., Zhong, S., Bian, X. and Liu, S. (2011) A North American Regional Reanalysis climatology of the Haines index. *International Journal of Wildland Fire*, 20, 91–103.

Mahrt, L. (2011) Surface wind direction variability. *Journal of Applied Meteorology and Climatology*, 50, 144–152. https://doi.org/10.1175/2010JAMC2560.1.

Mesinger, F., DiMego, G., Kalnay, E., Mitchell, K., Shafran, P.C., Ebisuzaki, W., Jovic, D., Woollen, J., Rogers, E., Berbery, E.H., Ek, M. B., Fan, Y., Grumbine, R., Higgins, W., Li, H., Lin, Y., Manikin, G., Parrish, D. and Shi, W. (2006) North American Regional Reanalysis. *Bulletin of the American Meteorological Society*, 87, 343–360.

Mesinger, F., Janjić, Z.I., Nicković, S., Gavrilov, D. and Deaven, D. G. (1988) The step-mountain coordinate: model description and performance for cases of Alpine lee cyclogenesis and for a case of an Appalachian redevelopment. *Monthly Weather Review*, 116, 1493–1518.

Mohan, M. and Siddiqui, T.A. (1998) Analysis of various schemes for the estimation of atmospheric stability classification. *Atmospheric Environment*, 32, 3775–3781.

Monroe, J. W. (2007) *Evaluating NARR surface reanalysis variables and NLDAS using Oklahoma Mesonet observations*. Master's thesis, University of Oklahoma, Norman, OK.

Muthama, N.J., Kaume, C.M., Mutai, B.K. and Ng'ang'a, J.K. (2015) Simulation of potential impact of air pollution from the proposed coal mining sites in Mui Basin, Kitui County, Africa. *Journal of Physical Science*, 2, 60–72.

Nadolski, V. L. (1998) *Automated Surface Observing System (ASOS) user's guide*. Available at: https://www.weather.gov/media/asos/aum-toc.pdf [Accessed 7th June 2021].

Novick, K., Biederman, J., Desai, A., Litvak, M., Moore, D., Scott, R. and Torn, M. (2018) The AmeriFlux network: a coalition of the willing. *Agricultural and Forest Meteorology*, 249, 444–456. https://doi.org/10.1016/j.agrformet.2017.10.009.

Pasquill, F. (1961) The estimation of the dispersion of windborne material. *Meteorological Magazine*, 90, 33–49.

Person, H. (2000) *Michigan odor print*. Available at: https://maeap.org/wp-content/uploads/2019/03/Michigan-Odor-Footprint.pdf [Accessed 7th June 2021].

Smith, A., Lott, N. and Vose, R. (2011) The integrated surface database: recent developments and partnerships. *Bulletin of the American Meteorological Society*, 92(6), 704–708. https://doi.org/10.1175/2011BAMS3015.1.

Stegall, S.T. and Zhang, J. (2012) Wind field climatology, changes, and extremes in the Chukchi-Beaufort Seas and Alaska North Slope during 1979–2009. *Journal of Climate*, 25, 8075–8089. https://doi.org/10.1175/JCLI-D-11-00532.1.

Stull, R.B. (1988) *An Introduction to Boundary Layer Meteorology*. Dordrecht, The Netherlands: Kluwer Academic.

Trubilowicz, J.W., Shea, J.M., Jost, G. and Moore, R.D. (2016) Suitability of North American Regional Reanalysis (NARR) output for hydrologic modelling and analysis in mountainous terrain. *Hydrological Processes*, 30, 2332–2347.

US EPA. (1993) *SCRAM surface meteorological archived data*. Washington, DC: US Environmental Protection Agency. Available at: https://www.epa.gov/scram/scram-surface-meteorological-archived-data [Accessed 9th July 2021].

Yu, L., Zhong, S. and Bian, X. (2017) Multi-day valley cold-air pools in the western United States as derived from NARR. *International Journal of Climatology*, 37, 2466–2476.

How to cite this article: Kiefer, M. T., Andresen, J. A., Rozeboom, D. W., & Bian, X. (2022). Development of a wind and Pasquill stability class climate dataset for the North American Great Lakes region. *International Journal of Climatology*, *42*(10), 5306–5320. https://doi.org/10.1002/joc.7534